Polyelectrolyte-Functionalized Graphene as Metal-Free Electrocatalysts for Oxygen Reduction

Shuangyin Wang,[†] Dingshan Yu,[†] Liming Dai,[†,*] Dong Wook Chang,[‡] and Jong-Beom Baek[‡]

[†]Department of Macromolecular Science and Engineering, Department of Chemical Engineering, Case Western Reserve University, Cleveland, Ohio 44106, United States, and [‡]Interdisciplinary School of Green Energy/Institute of Advanced Materials & Devices, Ulsan National Institute of Science and Technology (UNIST), 100 Banyeon, Ulsan, 689-798 South Korea

ABSTRACT Poly(diallyldimethylammonium chloride), PDDA, was used as an electron acceptor for functionalizing graphene to impart electrocatalytic activity for the oxygen reduction reaction (ORR) in fuel cells. Raman and X-ray photoelectron spectroscopic measurements indicate the charge transfer from graphene to PDDA. The resultant graphene positively charged *via* intermolecular charge-transfer with PDDA was demonstrated to show remarkable electrocatalytic activity toward ORR with better fuel selectivity, tolerance to CO posing, and long-term stability than that of the commercially available Pt/C electrode. The observed ORR electrocatalytic activity induced by the intermolecular charge-transfer provides a general approach to various carbon-based metal-free ORR catalysts for oxygen reduction.

KEYWORDS: graphene · PDDA · oxygen reduction reaction · fuel cells · charge transfer

Large-scale commercialization of fuel cells has been hindered largely by the slow kinetics characteristic of the cathodic oxygen reduction reaction (ORR).[1−6] Therefore, it is important to develop efficient electrocatalysts for ORR at the cathode in fuel cells and even metal−air batteries.[7−9] Traditionally, Pt-based nanomaterials have been used as active electrocatalysts for both anode and cathode in fuel cells. Although Pt nanomaterials have been regarded as the best electrocatalyst for ORR in fuel cells, they still suffer from multiple problems. For instance, Pt-based cathode electrocatalysts are susceptible to the crossover effect caused by the diffusion of fuel molecules from the anode through membrane to the cathode in fuel cells and CO poisoning.[1−6,10] Furthermore, the high cost of Pt, together with its limited reserve in nature, has been shown to be the "bottleneck" for large-scale commercialization of the fuel cell technology. Aiming at reducing the usage of the precious Pt metal and hence the cost of a fuel cell, the development of nonprecious metal or metal-free ORR electrocatalysts has thus generated a great deal of interest.[1,3,6,10−19]

In our previous effort on the development of metal-free ORR electrocatalysts,[20−23] we have found that vertically aligned nitrogen-doped carbon nanotubes (VA-NCNTs) produced by pyrolysis of iron(II) phthalocyanine could actively catalyze ORR *via* a four-electron process free from the crossover and CO poisoning effects with a 3-time higher electrocatalytic activity and better long-term durability than that of commercially available Pt/C electrocatalysts.[20] Similar ORR electrocatalytic activity was also observed for nitrogen-doped graphene (*N*-graphene).[21] On the basis of these experimental observations and quantum mechanics calculations,[20] we have attributed the observed ORR catalytic activities of the VA-NCNTs and *N*-graphene to the electron-accepting ability of the nitrogen atoms, which create a net positive charge (*via* intramolecular charge-transfer) on adjacent carbon atoms in the nanocarbon structures to readily attract electrons from the anode for facilitating the O_2 adsorption and the ORR process. These findings prompted us to develop carbon-based metal-free ORR catalysts in this study by positively charging carbon atoms in the nitrogen-free graphene plane through intermolecular charge-transfer. In particular, we found that physical adsorption of poly(diallyldimethylammonium chloride), PDDA, a positively charged polyelectrolyte with electron-withdrawing ability,[24,25] onto nitrogen-free graphene could create net positive charge on carbon-atoms in the all-carbon graphene plane *via* the intermolecular charge transfer (Scheme 1). The resultant PDDA-functionalized/adsorbed graphene was shown to possess dramatically enhanced electrocatalytic activities toward ORR.

In a typical experiment, the adsorption of PDDA onto the surface of graphene was performed during the process of reducing graphene oxide (GO) into graphene by sodium

* Address correspondence to liming.dai@case.edu.

Received for review March 6, 2011 and accepted July 22, 2011.

Published online July 22, 2011
10.1021/nn200879h

borohydride ($NaBH_4$) in the presence of PDDA.[26] Instead of using the conventional hydrazine, $NaBH_4$ was used as the reducing agent since hydrazine reduction often introduces nitrogen atoms into the graphene plane to produce N-doped graphene[27−29] that could show certain ORR activities[24] to interfere with the intermolecular charge-transfer effect. Upon $NaBH_4$ reduction, the color of the suspension changed from the yellow-brown of GO to black for graphene and PDDA−graphene (Figure 1a). Subsequent adsorption of PDDA made the surface of graphene positively charged, leading to a good dispersion *via* electrostatic repulsion among individual graphene sheets, which are also solubilized by the adsorbed PDDA chains. In the absence of PDDA, the $NaBH_4$-reduced graphene precipitates at the bottom of the vial (Figure 1a).

The reduction of GO and concomitant functionalization of the resultant graphene with PDDA were further followed by FTIR spectroscopic measurements. As shown in Figure 1a, the FTIR spectrum of GO shows a strong peak at around 1630 cm^{-1} attributable to aromatic C=C, along with peaks characteristic of C=O stretching (1720 cm^{-1}), carboxyl (1415 cm^{-1}), and epoxy (~1226 cm^{-1}).[30] The reduction of GO to graphene is evidenced by the dramatic decrease in peak intensity at ~1720, ~1415, and ~1226 cm^{-1}. Meanwhile, functionalization of graphene with PDDA is reflected by the appearance of new peaks at around ~850 and ~1505 cm^{-1}, attributable to the N−C bond in the adsorbed PDDA.

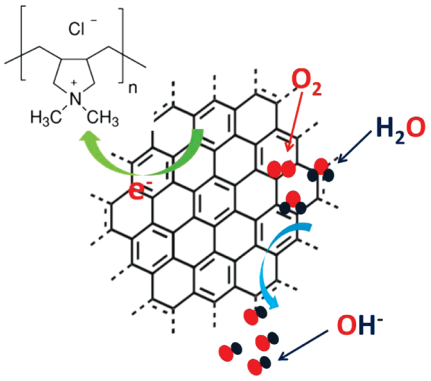

Scheme 1. Schematic illustration of the electron-withdrawing from graphene by PDDA to facilitate the ORR process.

Figure 1b shows thermogravimetric analysis (TGA) curves recorded under nitrogen for GO, graphene (*i.e.*, the $NaBH_4$-reduced GO), and PDDA−graphene. As can be seen, GO shows a relatively poor thermal stability with a rather low onset temperature for pyrolysis of the labile oxygen-containing functional groups over 180−300 °C.[31] The mass loss (~4 wt %) below 100 °C can be attributed to the removal of adsorbed water. The dramatically improved thermal stability of graphene indicates a successful reduction process. The PDDA−graphene shows a two-step thermal degradation process with about 15 wt % loss of PDDA up to around 500 °C.

Details of the chemical changes during the reduction of GO and functionalization with PDDA were further elucidated by X-ray photoelectron spectroscopic (XPS) measurements. Figure 2a shows XPS survey spectra for GO, graphene, and PDDA−graphene. As expected, the O/C atomic ratio significantly decreased upon the $NaBH_4$ reduction. Subsequent PDDA functionalization/adsorption caused further decrease in the O/C atomic ratio, which was accompanied by the appearance of N 1s and Cl 2p peaks located around 401.6 and 199.2 eV, respectively (Figure 2a).

The high-resolution C 1s XPS spectra for GO, graphene, and PDDA−graphene shown in Figure 2b−d can be fitted with four different components of oxygen-containing functional groups: (a) nonoxygenated C at 284.6 eV, (b) carbon in C−O at 285.6 eV, (c) epoxy carbon at 286.7 eV, and (d) carbonyl carbon (C=O, 288.2 eV). Compared with GO (Figure 2b), the graphene (Figure 2c) and PDDA−graphene (Figure 2d) samples showed a strong suppression for the oxygen-containing components of their C 1s XPS spectra. These results indicate efficient reduction of the oxygen-containing functional groups in GO by $NaBH_4$, particularly the

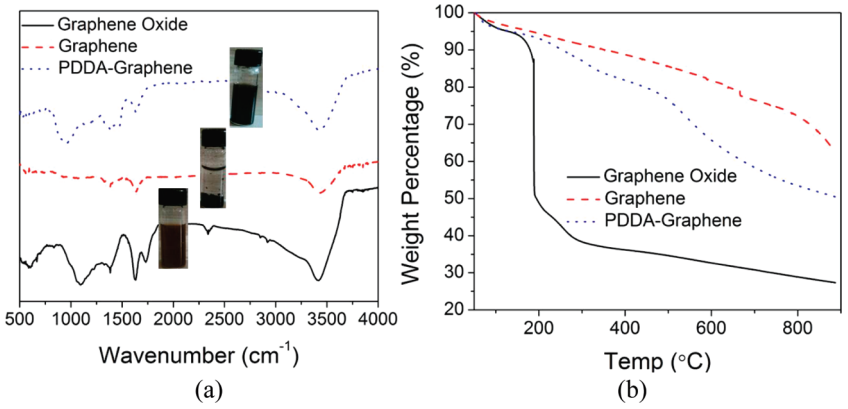

Figure 1. (a) FTIR spectra of graphene oxide, graphene, and PDDA-functionalized graphene. (b) TGA curves of graphene oxide, graphene, and PDDA−graphene at a heating rate of 10 °C/min under nitrogen atmosphere.

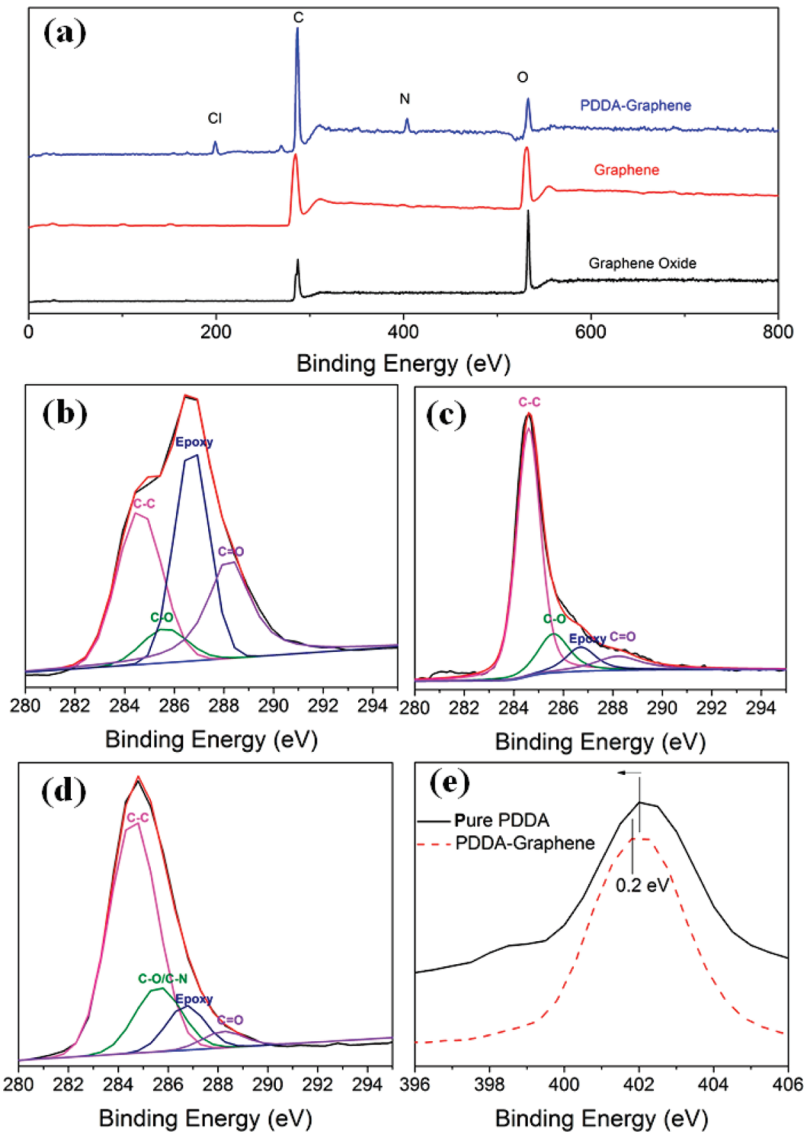

Figure 2. (a) XPS survey spectra for graphene oxide, graphene, and PDDA−graphene. The high resolution of C 1s XPS spectra of (b) graphene oxide, (c) graphene, and (d) PDDA−graphene. (e) The N 1s XPS spectra of PDDA−graphene and pure PDDA.

epoxy carbon, well consistent with the FTIR spectra shown in Figure 1a. Figure 2e shows the N 1s XPS spectra of the pure PDDA and PDDA−graphene. While the peak at ~402.0 eV for the pristine PDDA is attributable to the charged nitrogen (N^+), its negative shift to a lower binding energy (~401.8 eV) in PDDA−graphene indicates the electron transfer from graphene to the positively charged N^+ centers of PDDA.[16,35] Thus, PDDA has acted as a *p*-type dopant to cause the partial electron-transfer from the electron-rich graphene substrate.

The above observed intermolecular charge-transfer was also supported by Raman spectroscopic measurements.[32−34] Figure 3 shows the Raman spectra for graphene oxide, graphene, and PDDA−graphene. As expected, GO displays two prominent peaks at ~1585 and ~1351 cm^{-1} corresponding to the G and D bands, respectively. The D/G intensity ratio increased slightly from GO to graphene, suggesting a decrease of sp^2-domain induced by the $NaBH_4$ reduction.[41] Upon PDDA adsorption, the G band of graphene up-shifted from 1585 to 1594 cm^{-1}, indicating, once again, the occurrence of electron transfer from graphene to the adsorbed PDDA.[34,36] Similar G-band shifts caused by charge-transfer have been reported for graphene functionalized with other electron-accepting molecules.[36,37]

Like N-doped CNTs and N-graphene,[20,21] the charge transfer observed in PDDA−graphene could also impart electrocatalytic activities toward ORR for the nitrogen-free graphene. As such, we exploited the possibility of PDDA−graphene as novel metal-free catalysts for electrochemical reduction of O_2. The cyclic voltammograms (CVs) for oxygen reduction on the graphene and PDDA−graphene electrodes at a constant active mass loading (0.01 mg) in an aqueous O_2-saturated 0.1 M KOH solution are shown in Figure 4a. As

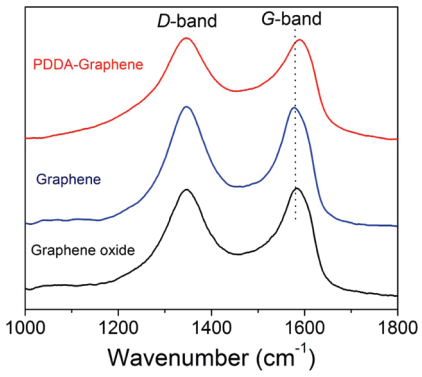

Figure 3. Raman spectra of graphene oxide, graphene, and PDDA–graphene.

can be seen, the onset potential of ORR for the pure graphene electrode is at −0.25 V (*versus* SCE) with the cathodic reduction peak around −0.47 V (*versus* SCE). Upon functionalization/adsorption of graphene with PDDA, both the onset potential and the ORR reduction peak potential shifted positively to around −0.15 and −0.35 V, respectively, accompanied by a concomitant increase in the peak current density (Figure 4a). These results clearly demonstrated a significant enhancement in the ORR electrocatalytic activity for the PDDA–graphene in respect to the pure graphene electrode.

To further investigate the ORR performance, we carried out the linear sweep voltammetric (LSV) measurements on a rotating disk electrode (RDE) with graphene and PDDA–graphene in an O_2-saturated 0.1 M KOH electrolyte solution. As shown in Figure 4b, the ORR at the bare graphene electrode commenced around −0.21 V (onset potential), whereas the ORR onset potential at the PDDA–graphene electrode significantly shifted positively to −0.12 V with the limiting diffusion current at −1.2 V being about 1.4 times stronger than that of the graphene electrode. However, the electrocatalytic activity of PDDA–graphene toward ORR in terms of the onset potential and current density is still not as good as that of the commercial Pt/C electrocatalyst (Figure 4b). Although the ORR electrocatalytic activity of the *as-prepared* (unoptimized) PDDA–graphene electrode is still lower than that of a commercial Pt/C electrode, the ease with which conventional *nitrogen-free* graphene materials can be converted into metal-free ORR electrocatalysts simply by the adsorption-induced *intermolecular charge-transfer* suggests considerable room for cost-effective preparation of various metal-free catalysts for ORR, and even new catalytic materials for applications beyond fuel cells (*e.g.,* metal-air batteries).

RDE voltammetry measurements were also carried out to gain further insight into the ORR performance of the graphene electrode before and after functionalization/adsorption with PDDA. Figure 5 panels a and b show the LSV curves at various different rotation rates

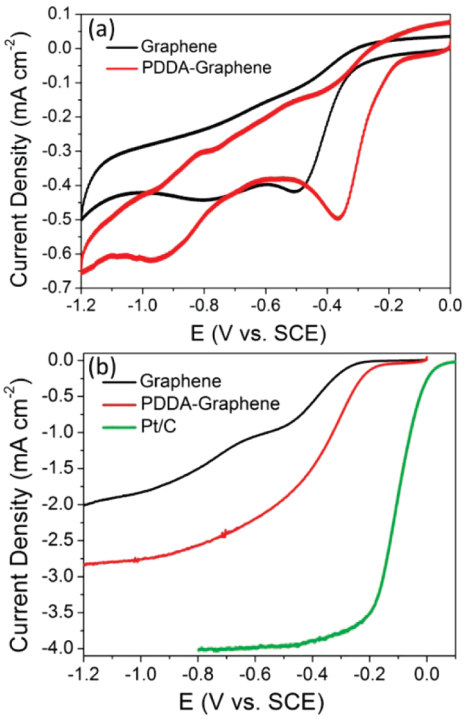

Figure 4. (a) CV curves of oxygen reduction on the graphene and PDDA–graphene electrodes in an O_2-saturated 0.1 M KOH solution at a scan rate of 50 mV s^{-1}. (b) LSV curves for oxygen reduction on the graphene, PDDA–graphene, and Pt/C electrodes in an O_2-saturated 0.1 M KOH solution at a scan rate of 10 mV s^{-1}.

for graphene and PDDA–graphene electrodes. As can be seen, adsorption of the hydrophilic PDDA chains, which facilitated interactions with the electrolyte, onto the graphene electrode (Figure 5a) led to the much better diffusion controlled regions shown in Figure 5b. The limiting current density increases with increasing rotation rate. At any constant rotation rate, the limiting current density of ORR at the PDDA–graphene electrode is always higher than that at the pure graphene electrode. The transferred electron numbers per O_2 involved in the oxygen reduction at both the graphene and PDDA–graphene electrodes were determined by the Koutechy–Levich equation as given below:[21,23]

$$\frac{1}{j} = \frac{1}{j_k} + \frac{1}{B\omega^{0.5}} \quad (1)$$

where j_k is the kinetic current and ω is the electrode rotating rate. B could be determined from the slope of the *K–L* plots (Figures 5c,d) based on the Levich equation as follows:[21]

$$B = 0.2nF(D_{O_2})^{2/3}\nu^{-1/6}C_{O_2} \quad (2)$$

where n represents the number of electrons transferred per oxygen molecule, F is the Faraday constant (F = 96485 C mol^{-1}), D_{O_2} is the diffusion coefficient of O_2 in 0.1 M KOH (1.9×10^{-5} cm^2 s^{-1}), ν is the kinetic viscosity (0.01 cm^2 s^{-1}), and C_{O_2} is the bulk concentration of O_2 (1.2×10^{-6} mol cm^{-3}). The constant 0.2 is adopted when the rotation speed is expressed in rpm.

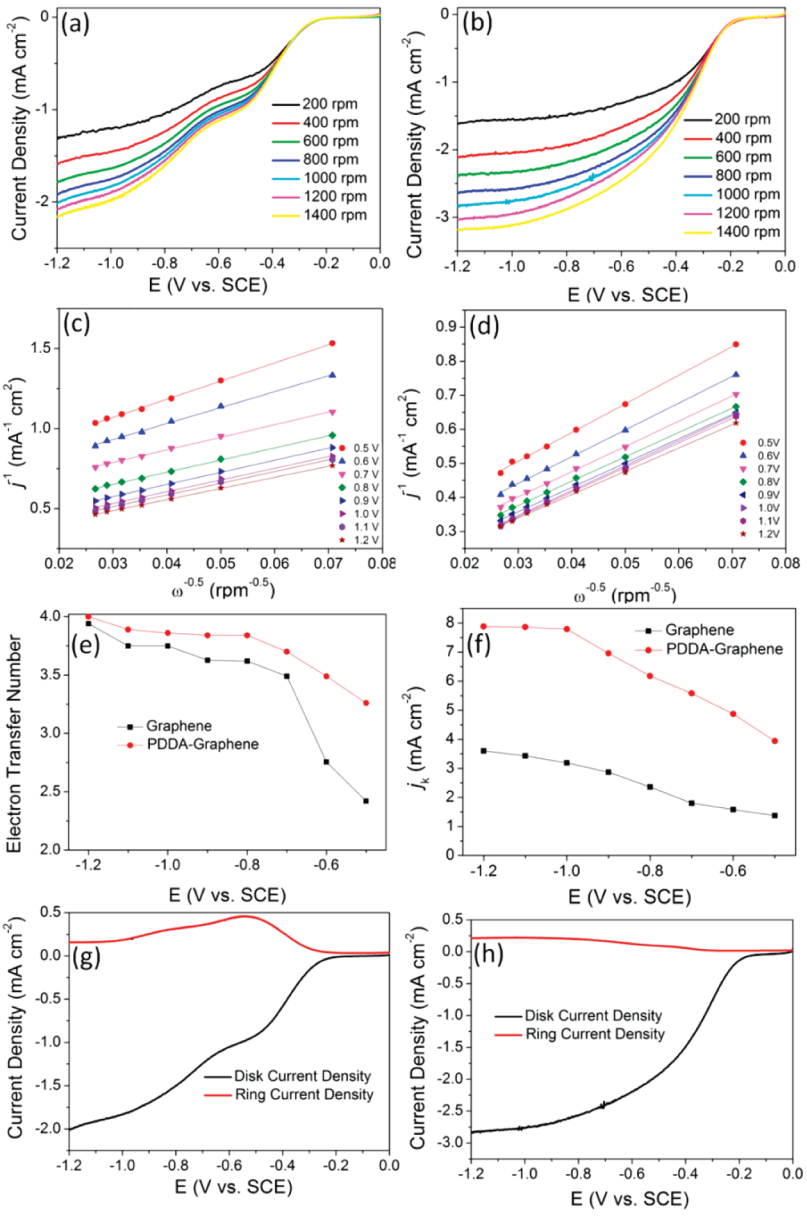

Figure 5. LSV curves at various different rotation rates for oxygen reduction at (a) the graphene and (b) PDDA–graphene electrode in an O_2-saturated 0.1 M KOH solution; *K–L* plots of ORR on (c) the graphene and (d) PDDA–graphene electrode. (e) The dependence of the electron transfer number and (f) the kinetic current density on the potential for both the graphene and PDDA–graphene electrodes. ORR on the RRDE of (g) the graphene and (h) PDDA–graphene electrode in an O_2-saturated 0.1 M KOH solution.

As shown in Figure 5 panels c and d, linear relationships between i^{-1} and $\omega^{-0.5}$ were observed for both the graphene and PDDA–graphene electrodes at various potentials. The number of electrons transferred per O_2 molecule (n) was calculated from the slope of the *K–L* plots, as shown in Figure 5e, in which the electron transfer number was found to be dependent on the potential for both the graphene and PDDA–graphene electrodes. In particular, the electron transfer number increased with a decrease in the negative potential. The electron transfer number for ORR at the PDDA–graphene electrode is always higher than that on the pure graphene electrode over the potential range covered in this study. Within the range of the electron transfer number from 3.5 to 4, the oxygen reduction reaction proceeds *via* a nearly four-electron pathway.[38,39] As seen in Figure 5e, the four-electron ORR reaction commenced at around −0.70 and −0.80 V on the PDDA–graphene and pure graphene electrode, respectively, indicating that PDDA–graphene is a more efficient ORR electrocatalyst than graphene. This is consistent with the relatively high calculated kinetic current density, j_k (eq 1), for ORR at the PDDA–graphene electrode with respect to the pure graphene electrode (Figure 5f). In addition, rotation ring-disk electrode (RRDE) was used to evaluate the ORR performance of the graphene and PDDA–graphene electrodes. Figures 5 panels g and h show

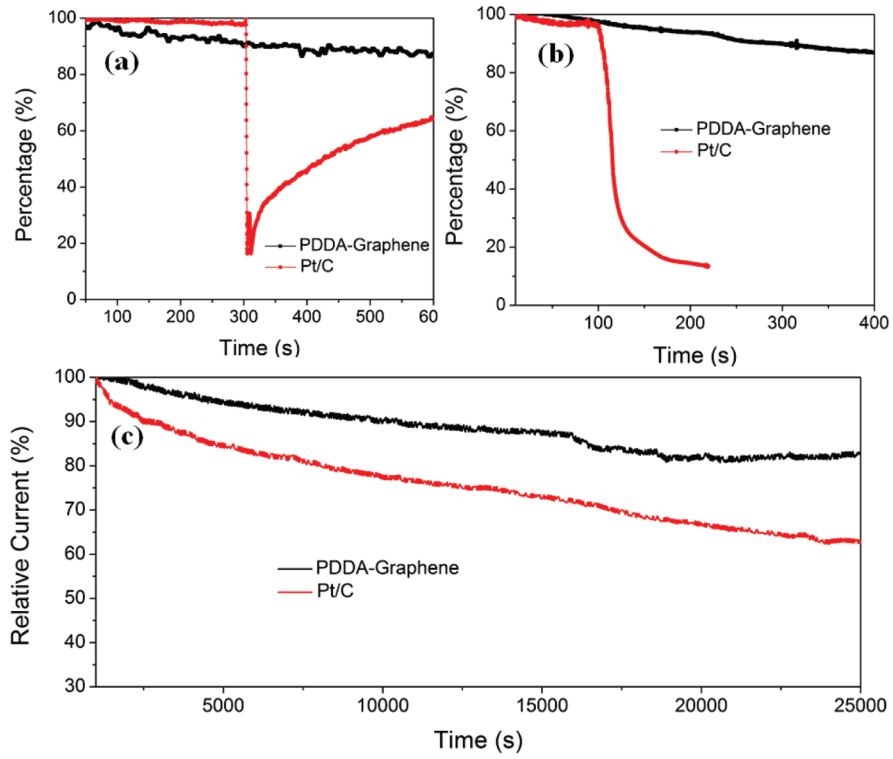

Figure 6. The current–time (*i*–*t*) chronoamperometric responses for ORR at the PDDA–graphene and Pt/C electrodes in an O_2-saturated 0.1 M KOH solution at −0.4 V *versus* SCE: (a) 3.0 M methanol was added at around 300 s and (b) CO was added at around 100 s, and (c) at −0.28 V *versus* SCE at a rotation rate of 1000 rpm.

the disk and ring currents for the graphene and PDDA–graphene electrode, respectively. The ring currents were measured to estimate the amount of generated hydrogen peroxide ions.[20,21] As can be seen, both of the electrodes started to generate the ring current at the onset potential for oxygen reduction. However, the amount of hydrogen peroxide ions generated on the PDDA–graphene electrode is significantly less than that on the pure graphene, indicating that PDDA–graphene is a more efficient ORR electrocatalyst. The electron transferred number (*n*) of ORR on graphene and PDDA–graphene estimated from the ring and disk currents[20] (see Supporting Information) at −0.5 V are found to be around 1.5 and 3.5, respectively, which are consistent with the *K*–*L* analyses.

The PDDA–graphene electrode was further subjected to testing the possible crossover and the stability toward ORR. To examine the possible crossover effect in the presence of other fuel molecules (*e.g.,* methanol) and the poisoning effect by carbon monoxide (CO), the current–time (*i*–*t*) chronoamperometric responses for ORR at the PDDA–graphene and Pt/C electrodes were obtained (Figures 6a,b). As shown in Figure 6a, a sharp decrease in current was observed for the Pt/C electrode upon addition of 3.0 M methanol. However, the corresponding amperometric response for the PDDA–graphene electrode remained almost unchanged even after the addition of methanol. This result unambiguously indicates that the PDDA–graphene electrocatalyst has higher fuel selectivity toward ORR than the commercial Pt/C electrocatalyst. To examine the effect of CO poisoning on the electrocatalytic activities of the PDDA–graphene and Pt/C electrodes, a CO gas was introduced into the electrolyte. As seen in Figure 6b, the PDDA–graphene electrode was insensitive to CO, whereas the Pt/C electrode was rapidly poisoned under the same conditions.

Finally, the durability of the PDDA–graphene and commercial Pt/C electrodes for ORR was evaluated *via* a chronoamperometric method at −0.28 V in an O_2-saturated 0.1 M KOH at a rotation rate of 1000 rpm. As seen in Figure 6c, the current density from both the PDDA–graphene and Pt/C electrodes initially decreased with time. However, the PDDA–graphene electrode exhibited a much slower decrease than the Pt/C electrode and leveled off after continuous reaction for about 17000 s, indicating that the PDDA–graphene electrocatalyst is much more stable than the commercial Pt/C electrode.

In summary, we have demonstrated that certain polyelectrolyte (*e.g.,* PDDA) functionalized/adsorbed graphene could act as an efficient metal-free electrocatalyst through intermolecular charge-transfer that creates net positive charge on carbon atoms in the nitrogen-free graphene plane to facilitate the ORR catalytic activity. Notably, the PDDA-adsorbed graphene electrode shows remarkable ORR electrocatalytic activities with a better fuel selectivity, more tolerance to CO

posing, and higher long-term stability than that of commercially available Pt/C electrode. While further work, including theoretical calculation, is needed to fully understand the ORR mechanism induced by the intermolecular charge transfer, we believe that the active site for ORR is still carbon atoms in the graphene sheets with the adsorbed PDDA to create somewhat *delocalized* positive charges on the conjugated carbon surface of graphene to alter the electronic properties of graphene and its adsorption behavior toward oxygen for facilitating the ORR process. Although the electrocatalytic activity of PDDA–graphene is not as good as that of nitrogen-doped carbon nanotubes and Pt/C, the ease with which graphene materials can be produced by various low-cost large-scale methods, including the chemical vapor deposition, chemical reduction of graphite oxide, and exfoliation of graphite, suggests considerable room for cost-effective preparation of metal-free efficient graphene-based catalysts for oxygen reduction. These findings indicate that the intermolecular charge-transfer can serve as a general approach to the cost-effective development of various carbon-based metal-free efficient ORR catalysts.

METHODS

Synthesis of Graphene Oxide. Graphene oxide (GO) was synthesized from natural graphite powder according to a modified Hummers method.[28,36,40–42] Briefly, 0.9 g of graphite powder was added into a mixture of 7.2 mL of 98% H_2SO_4, 1.5 g of $K_2S_2O_8$, and 1.5 g of P_2O_5. The solution was kept at 80 °C for 4.5 h, followed by thorough washing with water. Thereafter, the as-treated graphite was put into a 250 mL beaker, to which 0.5 g of $NaNO_3$ and 23 mL of H_2SO_4 (98%) were then added while keeping the beaker in the ice bath. Subsequently, 3 g of $KMnO_4$ was added slowly. After 5 min, the ice bath was removed and the solution was heated up to and kept at 35 °C under vigorous stirring for 2 h, followed by the slow addition of 46 mL of water. Finally, 40 mL of water and 5 mL of H_2O_2 was added, followed by water washing and filtration. The exfoliation of graphene oxide was then performed by ultrasonication (Fisher-Scientific Mechanical Cleaner FS110, 50/60 Hz, 185w).

Synthesis of PDDA Functionalized/Adsorbed Graphene. PDDA functionalized/adsorbed graphene (PDDA–graphene) was prepared by sodiumborohydride ($NaBH_4$) reduction of GO in the presence of PDDA. Briefly, GO (100 mg) was loaded in a 250-mL round-bottom flask, followed by the addition of 100 mL of PDDA (0.5 wt %) in water to produce an inhomogeneous yellow-brown dispersion. This dispersion was sonicated until it became clear with no visible particulate and kept under stirring for overnight. Thereafter, 100 mg of $NaBH_4$ was added and the solution was stirred for 30 min, followed by heating in an oil bath at 130 °C equipped with a water-cooling condenser for 3 h to produce a homogeneous black suspension. The final product (PDDA–graphene) was collected through filtration and dried in a vacuum oven for 24 h. To obtain the unfunctionalized graphene, the above procedure was adopted in the absence of PDDA.

Characterization. Electrochemical measurements were performed using a computer-controlled potentiostat (CHI 760C, CH Instrument, USA) with a typical three-electrode cell. A platinum wire was used as counter-electrode and saturated calomel electrode (SCE) as reference electrode. All the experiments were conducted at room temperature (25 ± 1 °C). For the electrode preparation, graphene or PDDA–graphene suspension in ethanol (1 mg/mL) was prepared by introducing a predetermined amount of the corresponding graphene sample in ethanol under sonication. A 10 μL portion of the graphene or PDDA–graphene suspension was then dropped onto the surface of a prepolished glassy carbon electrode (GCE), followed by dropping 5 μL of Nafion solution in isopropyl alcohol (0.5 wt %) as a binder. For a comparison, Pt/C electrode was also prepared: Pt/C suspension was prepared by dispersing 10 mg of Pt/C powder in 10 mL of ethanol in the presence of 50 μL of 5% Nafion solution in isopropyl alcohol. The addition of a small amount of Nafion could effectively improve the dispersion of the Pt/C catalyst suspension.[43]

X-ray photoelectron spectroscopic (XPS) measurements were performed on a VG Microtech ESCA 2000 instrument using a monochromic Al X-ray source (97.9 W, 93.9 eV). Thermogravimetric analyses were carried out on a TA instruments with a heating rate of 10 °C under N_2. FTIR measurements were performed on a FTIR spectroscope (PerkinElmer). Raman spectra were collected with a Renishaw inVita Raman spectrometer with an excitation wavelength of 514.5 nm. SEM images were recorded on a Hitachi S4800-F scanning electron microscope.

Acknowledgment. The authors acknowledge the support from the NSF (CMMI-1000768; CMS-1047655), AFOSR (FA9550-09-1-0331, FA2386-10-1-4071, FA9550-10-1-0546), and WCU and US-Korea NBIT Projects through UNIST from the Ministry of Education, Science and Technology in Korea.

Supporting Information Available: Additional TGA and electrochemical results. This material is available free of charge *via* the Internet at http://pubs.acs.org.

REFERENCES AND NOTES

1. Peng, Z.; Yang, H. Synthesis and Oxygen Reduction Electrocatalytic Property of Pt-on-Pd Bimetallic Heteronanostructures. *J. Am. Chem. Soc.* **2009**, *131*, 7542–7543.
2. Shao, M.-H.; Sasaki, K.; Adzic, R. R. Pd–Fe Nanoparticles as Electrocatalysts for Oxygen Reduction. *J. Am. Chem. Soc.* **2006**, *128*, 3526–3527.
3. Stamenkovic, V. R.; Fowler, B.; Mun, B. S.; Wang, G. J.; Ross, P. N.; Lucas, C. A.; Markovic, N. M. Improve Oxygen Reduction Activity on $Pt_3Ni(111)$ *via* Increased Surface Site Availability. *Science* **2007**, *315*, 493–497.
4. Wang, D.; Lu, S.; Jiang, S. P. Pd/HPW-PDDA-MWCNTs as Effective Non-Pt Electrocatalysts for Oxygen Reduction Reaction of Fuel Cells. *Chem. Commun.* **2010**, *46*, 2058–2060.
5. Xiao, L.; Zhuang, L.; Liu, Y.; Lu, J. T.; Abruna, H. D. Activating Pd by Morphology Tailoring for Oxygen Reduction. *J. Am. Chem. Soc.* **2009**, *131*, 602–608.
6. Zhang, J. D.; Vukmirovic, M. R.; Xu, Y.; Mavrikakis, M.; Adzic, R. R. Controlling the Catalytic Activity of Platinum-Monolayer Electrocatalysts for Oxygen Reduction with Different Substrates. *Angew. Chem., Int. Ed.* **2005**, *44*, 2170–2173.
7. Zhang, M. N.; Yan, Y. M.; Gong, K. P.; Mao, L. Q.; Guo, Z. X.; Chen, Y. Electrostatic Layer-by-Layer Assembled Carbon Nanotube Multilayer Film and Its Electrocatalytic Activity for O_2 Reduction. *Langmuir* **2004**, *20*, 8781–8785.
8. Alexeyeva, N.; Tammeveski, K. Electroreduction of Oxygen on Gold Nanoparticle/PDDA–MWCNT Nanocomposites in Acid Solution. *Anal. Chim. Acta* **2008**, *618*, 140–146.
9. Liu, Z.; Koh, S.; Yu, C.; Strasser, P. Synthesis, Dealloying, and ORR Electrocatalysis of PDDA-Stabilized Cu-Rich Pt Alloy Nanoparticles. *J. Electrochem. Soc.* **2007**, *154*, B1192–B1199.
10. Wu, G.; More, K. L.; Johnston, C. M.; Zelenay, P. High-Performance Electrocatalysts for Oxygen Reduction Derived

from Polyaniline, Iron, and Cobalt. *Science* **2011**, *332*, 443–447.
11. Hwang, B. J.; Kuma, S. M. S.; Chen, C.; Monalisa; Cheng, M.; Liu, D.; Lee, J. An Investigation of Structure-Catalytic Activity Relationship for Pt-Co/C Bimetallic Nanoparticles Toward the Oxygen Reduction Reaction. *J. Phys. Chem. C* **2007**, *111*, 15267–15276.
12. Yang, W.; Wang, Y.; Li, J.; Yang, X. Polymer Wrapping Technique: An Effective Route to Prepare Pt Nanoflower/Carbon Nanotube Hybrids and Application in Oxygen Reduction. *Energy Environ. Sci.* **2010**, *3*, 144–149.
13. Wang, S.; Jiang, S.; White, T. J.; Guo, J.; Wang, X. Electrocatalytic Activity and Interconnectivity of Pt Nanoparticles on Multiwalled Carbon Nanotubes for Fuel Cells. *J. Phys. Chem. C* **2009**, *113*, 18935–18945.
14. Wang, S.; Jiang, S. P.; Wang, X. Polyelectrolyte Functionalized Carbon Nanotubes as a Support for Noble Metal Electrocatalysts and Their Activity for Methanol Oxidation. *Nanotechnology* **2008**, *19*, 265601.
15. Wang, S.; Jiang, S. P.; White, T. J.; Wang, X. Synthesis of Pt and Pd Nanosheaths on Multiwalled Carbon Nanotubes as Potential Electrocatalysts of Low Temperature Fuel Cells. *Electrochim. Acta* **2010**, *55*, 7652–7658.
16. Wang, S.; Yang, F.; Jiang, S. P.; Chen, S.; Wang, X. Tuning the Electrocatalytic Activity of Pt Nanoparticles on Carbon Nanotubes *via* Surface Functionalization. *Electrochem. Commun.* **2010**, *12*, 1646–1649.
17. Wang, S. Y.; Kristian, N.; Jiang, S. P.; Wang, X. Controlled Deposition of Pt on Au Nanorods and Their Catalytic Activity Towards Formic Acid Oxidation. *Electrochem. Commun.* **2008**, *10*, 961–964.
18. Wang, S. Y.; Kristian, N.; Jiang, S. P.; Wang, X. Controlled Synthesis of Dendritic Au@Pt Core−Shell Nanomaterials for Use as an Effective Fuel Cell Electrocatalyst. *Nanotechnology* **2009**, *20*, 25605.
19. Wang, S. Y.; Wang, X.; Jiang, S. P. PtRu Nanoparticles Supported on 1-Aminopyrene-Functionalized Multiwalled Carbon Nanotubes and Their Electrocatalytic Activity for Methanol Oxidation. *Langmuir* **2008**, *24*, 10505–10512.
20. Gong, K. P.; Du, F.; Xia, Z. H.; Durstock, M.; Dai, L. M. Nitrogen-Doped Carbon Nanotube Arrays with High Electrocatalytic Activity for Oxygen Reduction. *Science* **2009**, *323*, 760–764.
21. Qu, L. T.; Liu, Y.; Baek, J. B.; Dai, L. M. Nitrogen-Doped Graphene as Efficient Metal-free Electrocatalyst for Oxygen Reduction in Fuel Cells. *ACS Nano* **2010**, *4*, 1321–1326.
22. Xiong, W.; Du, F.; Liu, Y.; Perez, A.; Supp, M.; Ramakrishnan, T. S.; Dai, L.; Jiang, L. 3-D Carbon Nanotube Structures Used as High Performance Catalyst for Oxygen Reduction Reaction. *J. Am. Chem. Soc.* **2010**, *132*, 15839–15841.
23. Yu, D.; Zhang, Q.; Dai, L. Highly Efficient Metal-free Growth of Nitrogen-Doped Single-Walled Carbon Nanotubes on Plasma-Etched Substrates for Oxygen Reduction. *J. Am. Chem. Soc.* **2010**, *132*, 15127–15129.
24. Yang, D. Q.; Rochette, J. F.; Sacher, E. Spectroscopic Evidence for $\pi-\pi$ Interaction between Poly(diallyl dimethylammonium) Chloride and Multiwalled Carbon Nanotubes. *J Phys. Chem. B* **2005**, *109*, 4481–4484.
25. Wang, S.; Yu, D.; Dai, L. Polyelectrolyte Functionalized Carbon Nanotubes as Efficient Metal-free Electrocatalysts for Oxygen Reduction. *J. Am. Chem. Soc.* **2011**, *133*, 5182–5185.
26. Shen, J.; Hu, Y.; Shi, M.; Lu, X.; Qin, C.; Li, C.; Ye, M. Fast and Facile Preparation of Graphene Oxide and Reduced Graphene Oxide Nanoplatelets. *Chem. Mater.* **2009**, *21*, 3514–3520.
27. Eda, G.; Fanchini, G.; Chhowalla, M. Large-Area Ultrathin Films of Reduced Graphene Oxide as a Transparent and Flexible Electronic Material. *Nat. Nanotechnol.* **2008**, *3*, 270–274.
28. Gao, X.; Jang, J.; Nagase, S. Hydrazine and Thermal Reduction of Graphene Oxide: Reaction Mechanisms, Product Structures, and Reaction Design. *J. Phys. Chem. C* **2009**, *114*, 832–842.
29. Stankovich, S.; Dikin, D. A.; Piner, R. D.; Kohlhaas, K. A.; Kleinhammes, A.; Jia, Y.; Wu, Y.; Nguyen, S. T.; Ruoff, R. S. Synthesis of Graphene-Based Nanosheets *via* Chemical Reduction of Exfoliated Graphite Oxide. *Carbon* **2007**, *45*, 1558–1565.
30. Liu, K.; Zhang, J.; Yang, G.; Wang, C.; Zhu, J.-J. Direct Electrochemistry and Electrocatalysis of Hemoglobin Based on Poly(diallyldimethylammonium chloride) Functionalized Graphene Sheets/Room Temperature Ionic Liquid Composite Film. *Electrochem. Commun.* **2010**, *12*, 402–405.
31. Zu, S.-Z.; Han, B.-H. Aqueous Dispersion of Graphene Sheets Stabilized by Pluronic Copolymers: Formation of Supramolecular Hydrogel. *J. Phys. Chem. C* **2009**, *113*, 13651–13657.
32. Jang, J.-H.; Rangappa, D.; Kwon, Y.-U.; Honma, I. Direct Preparation of 1-PSA Modified Graphene Nanosheets by Supercritical Fluidic Exfoliation and Its Electrochemical Properties. *J. Mater. Chem.* **2011**, *21*, 3462–3466.
33. He, P.; Bayachou, M. Layer-by-Layer Fabrication and Characterization of DNA-Wrapped Single-Walled Carbon Nanotube Particles. *Langmuir* **2005**, *21*, 6086–6092.
34. Rao, A. M.; Eklund, P. C.; Bandow, S.; Thess, A.; Smalley, R. E. Evidence for Charge Transfer in Doped Carbon Nanotube Bundles from Raman Scattering. *Nature* **1997**, *388*, 257–259.
35. Panchakarla, L. S.; Subrahmanyam, K. S.; Saha, S. K.; Govindaraj, A.; Krishnamurthy, H. R.; Waghmare, U. V.; Rao, C. N. R. Synthesis, Structure, and Properties of Boron- and Nitrogen-Doped Graphene. *Adv. Mater.* **2009**, *21*, 4726–4730.
36. Qi, X.; Pu, K.-Y.; Zhou, X.; Li, H.; Liu, B.; Boey, F.; Huang, W.; Zhang, H. Conjugated-Polyelectrolyte-Functionalized Reduced Graphene Oxide with Excellent Solubility and Stability in Polar Solvents. *Small* **2010**, *6*, 663–669.
37. Hsiao, M.-C.; Liao, S.-H.; Yen, M.-Y.; Liu, P.-I.; Pu, N.-W.; Wang, C.-A.; Ma, C.-C. M. Preparation of Covalently Functionalized Graphene Using Residual Oxygen-Containing Functional Groups. *ACS Appl. Mater. Interfaces* **2010**, *2*, 3092–3099.
38. Jurmann, G.; Tammeveski, K. Electroreduction of Oxygen on Multiwalled Carbon Nanotubes Modified Highly Oriented Pyrolytic Graphite Electrodes in Alkaline Solution. *J. Electroanal. Chem.* **2006**, *597*, 119–126.
39. Liu, R. L.; Wu, D. Q.; Feng, X. L.; Mullen, K. Nitrogen-Doped Ordered Mesoporous Graphitic Arrays with High Electrocatalytic Activity for Oxygen Reduction. *Angew. Chem., Int. Ed.* **2010**, *49*, 2565–2569.
40. Yoo, E.; Okata, T.; Akita, T.; Kohyama, M.; Nakamura, J.; Honma, I. Enhanced Electrocatalytic Activity of Pt Subnanoclusters on Graphene Nanosheet Surface. *Nano Lett.* **2009**, *9*, 2255–2259.
41. Zhang, L. L.; Zhou, R.; Zhao, X. S. Graphene-Based Materials as Supercapacitor Electrodes. *J. Mater. Chem.* **2010**, *20*, 5983–5992.
42. Hummers, W. S.; Offeman, R. E. Preparation of Graphitic Oxide. *J. Am. Chem. Soc.* **1958**, *80*, 1339–1339.
43. Cheng, S. A.; Liu, H.; Logan, B. Power Densities Using Different Cathode Catalysts (Pt and CoTMPP) and Polymer Binders (Nafion and PTFE) in Single Chamber Microbial Fuel Cells. *Environ. Sci. Technol.* **2006**, *40*, 364–369.